2007-03-01

Performance Characteristics of a Therapeutic Ultrasound Wire Waveguide

Graham Gavin
Dublin Institute of Technology, graham.gavin@dit.ie

Garrett McGuinness
Dublin City University

Finbar Dolan
Medtronic Vascular

M.S. Hashmi
Dublin City University

Performance Characteristics of a Therapeutic Ultrasound Wire Waveguide Apparatus

Graham P. Gavin[1]*, Garrett B. McGuinness[1], Finbar Dolan[2], M.S.J. Hashmi[1]

1. *School of Mechanical and Manufacturing Engineering, Dublin City University, Dublin, Ireland*

2. *Medtronic Vascular, Galway, Ireland*

* *Corresponding Author; Current Address: School of Mechanical and Manufacturing Engineering, Dublin City University, Glasnevin, Dublin, Ireland, Tel: +35317005712,*

Email: graham.gavin@dcu.ie

Abstract

Therapeutic ultrasound angioplasty has been investigated, clinically, by a number of researchers and represents a potentially promising therapy, for the treatment of atherosclerotic lesions. To date, there has been no detailed analysis of the mechanical design and the effect of parameters, such as length and damping, for example, on wire waveguide performance characteristics. In this work, an apparatus capable of delivering therapeutic ultrasound down small diameter nickel-titanium (NiTi) wire waveguides is described. The output peak-to-peak (p-p) displacements at the distal tip of a 1.0 mm diameter wire waveguide were measured experimentally, by means of an optical microscope and image analysis software. The apparatus was tested for a range of wire waveguide lengths from 118 mm to 303 mm. Wire waveguide distal tip displacements as high as 98μm (p-p) at 23.5 kHz were measured. For the range of lengths tested, the experimental measurements show the critical relationship between output distal tip displacements and lengths of waveguide where resonance occurs. The finite element model developed that can determine the resonant lengths and achievable distal tip displacements of the wire waveguide, with the inclusion of a validated damping constant, will be a valuable design tool for therapeutic ultrasound angioplasty. This numerical model has been validated against the experimental displacement data obtained.

Nomenclature:

l	=	length of wire waveguide
c	=	longitudinal speed of sound in material
f	=	frequency of ultrasound
β	=	matrix stiffness multiplier
ζ	=	constant damping value
$[M]$	=	mass matrix
$[C]$	=	damping matrix
$[K]$	=	stiffness matrix
$(\ddot{u})$	=	nodal acceleration vector
$(\dot{u})$	=	nodal velocity vector
(u)	=	nodal displacement vector
(F^a)	=	applied load vector.

1. Introduction

The use of ultrasound in medicine is well documented, for both its diagnostic and therapeutic capabilities. In cardiology, intravascular diagnostic imaging is used to identify the presence, severity and composition of atherosclerotic lesions. Therapeutic ultrasound has been used in the treatment of kidney stones and in aortic valve de-calcification [1]. It has been proposed that this technology makes use of the fact that at low-ultrasonic frequencies and high-amplitude displacements, inelastic rigid tissue is disrupted, while healthier elastic tissue can remain largely unaffected [2].

It has been hypothesised that in cardiovascular surgery, this form of energy may prove extremely beneficial in the treatment of calcified atherosclerotic plaques [1]. Calcified lesions pose a considerable problem to present procedures, such as balloon angioplasty and stent implantation, which both rely on the mechanical loading of the plaque to re-open the occluded artery. The rigid behaviour of the calcified plaque

can often resist this loading and in many cases, higher balloon inflation pressures have to be utilised. Siegel *et al* [3] propose a link between high balloon inflation pressures and deep vessel injuries and acute complications, known as 'barotraumas'. Topoleski and Salunke [4] have shown that the rigidity of the calcified material may require more specific protocols to induce fracture in the material, either prior to or during conventional interventions or as a stand alone procedure.

The development and *in vivo* testing of apparatuses that could deliver therapeutic ultrasound to a lesion began in the early 1970's, when Sobbe *et al* [5, cited in 1] delivered ultrasonic vibrations via a wire probe, resulting in the disruption of blood clots in animals. During the mid-1980's particular design issues were addressed by numerous investigators to improve the ultrasound delivery methods [6- 10]. Siegel *et al* [6] and Rosenschein *et al* [7] describe the generation of ultrasound external of the body by means of a piezoelectric transducer and ultrasonic generator. These transducers convert electrical energy to longitudinal mechanical displacements and when driven by an ultrasonic generator, can output axial displacements as high as 10 μm peak-to-peak (p-p) at between 18-45 kHz.

These displacements are then further amplified by means of an acoustic horn attached to the front mass of the transducer. An acoustic horn is a solid metal rod, designed to resonate longitudinally, at the same frequency as the transducer and is often tapered or stepped to further amplify the ultrasonic waves as they travel through the horn. Titanium or aluminium alloys are commonly used in the manufacture of acoustic horns and axial displacements as high as 150 μm (p-p) have been documented [7].

Most work has concentrated on the delivery of this form of energy through the tortuous vascular structure to the lesion location. Rosenschein *et al* [7] describe the use of a 1.6 mm diameter solid aluminium transmission wire coupled directly to the acoustic horn. Fischell *et al* [8] working on an apparatus developed by Siegel and colleagues describes the use of a 0.5 mm diameter titanium wire waveguide. This system also appears to have been used by Ariani *et al* [9] and Demer *et al* [10]. US Patent *5304115* (1994) claims that a wire manufactured from Nickel-Titanium (NiTi) alloy may prove beneficial [11]. In their austenitic phase, these alloys appear to be able to, both, transmit ultrasound and due to their superelastic behavior, have the flexibility to navigate through the arterial structure.

Once coupled to the radiating face of the acoustic horn, the longitudinal ultrasonic waves are delivered into the wire waveguide and manifest themselves as a distal tip axial peak-to-peak displacement.

This can result in numerous mechanisms thought to be responsible for the disruption of atherosclerotic plaques or rigid material. Atar *et al* [12] concluded that four main mechanisms, as shown in *Figure 1*, are responsible for plaque disruption: 1) *direct contact*, 2) *cavitation*, 3) *acoustic micro-streaming* and 4) *pressure wave components*. All these mechanisms are directly related to the distal tip displacement, amplitude and frequency.

Ariani *et al* [9] describe a method for measuring the peak-to-peak output displacement at the distal tip of the wire waveguide, by the use of an optical microscope. In this configuration, the microscope is focused on the distal tip of the wire waveguide. When the ultrasound is applied to the transmission wire, the distal tip is streaked across the image and the output peak-to-peak displacement can be measured.

Rosenschein *et al* [2] and Demer *et al* [10] reported favourable results when *in vivo* and *in vitro* tests were performed on calcified atherosclerotic material. It would appear from these results and those of Siegel [3] that therapeutic ultrasound angioplasty is capable of ablating calcified and fibrous lesions, while avoiding damage to the healthy flexible arterial wall.

The majority of work, to date, appears to be focused on assessing the end clinical results of the delivery of the therapeutic ultrasound, with little information regarding how the ultrasound is transmitted to the distal tip of wire waveguides, or how it is affected by various waveguide parameters. This work seeks to further understand how ultrasound is delivered to the distal location and how resonance and damping in the waveguide may affect the output distal tip displacements.

This is achieved by developing a therapeutic wire waveguide apparatus capable of delivering ultrasonic longitudinal displacements at an amplitude and frequency similar to those reported in the literature. The apparatus is tested to determine the wire waveguide distal tip displacements (p-p) for a wide range of lengths of a 1.0mm diameter waveguide.

In addition, the finite element method is used to simulate the wire waveguide behaviour, to determine the frequency of operation, resonant lengths and distal tip peak-to-peak displacements. This model is validated against the experimental data obtained.

2. Experimental Methods

2.1. *Therapeutic Ultrasound Waveguide Apparatus*

Design requirements were established for the ultrasound wire waveguide apparatus based on work reported in the literature [2,3,7 and 9]. These requirements included frequency of operation, achievable output displacements and wire waveguide diameter.

The actual experimental apparatus consists of a piezoelectric converter and titanium alloy acoustic horn that operates with a resonant frequency of approximately 23.5 kHz, as shown in *Figure 2*. The converter is driven by an ultrasonic generator at the resonant frequency, although the generator is also capable of auto-tuning by sweeping through ± 6 % of this value. This ensures that resonance of the acoustic horn is achieved despite minor alterations in the resonant frequency of the system. In addition, the generator has adjustable input power dial settings and can display the overall root-mean-square power delivered to the distal tip of the acoustic horn.

The 1.0 mm diameter wire waveguide is made from a nickel-titanium alloy (56.0 wt % Ni, Balance Ti), which exhibits superelastic properties above approximately -10 degrees Celsius. In order to connect the waveguide to the acoustic horn, an axial crimp screw is used. The wire waveguide is crimped into the screw and both are fixed tightly into the radiating face of the acoustic horn. This ensures a rigid connection between the wire waveguide and the horn.

As the converter is adapted from sonochemistry applications and the acoustic horn is a tapered micro-horn it is necessary to encase the horn and connector to allow for infusion of a fluid to cool and load the horn. The entire apparatus is housed in a lightweight portable unit, with the wire waveguide emerging ensheathed in a catheter.

2.2. *Experimental Analysis of Apparatus*

Distal tip peak-to-peak displacements of the wire waveguide were measured experimentally by means of an optical microscope *(SPS Laboratories)*, digital colour camera *(Vantage)* and image analysis software *(Image Analysis System, Buehler)*. With a magnification factor of 40, the distal tip of the wire waveguide was focused on and energised with the ultrasound. This process results in a streaked image (the

distal tip peak-to-peak displacement of the vibrating wire waveguide) being captured and sent to the image analysis software where the length of the streak was measured.

This process was performed for four input power dials settings of 1.5, 2, 2.25 and 2.5, corresponding to acoustic horn distal tip power levels of 10, 13, 15 and 17 Watts (RMS) respectively, on wire waveguides over a range of lengths. The lengths of wire tested were from 118 mm to 303 mm in increments of 5 mm.

3. Numerical Methodology

The problem sketch for the wire waveguide is shown in *Figure 3a*, while the corresponding meshed model is shown in *Figure 3b*. The wire waveguide was modelled as a thin rod, using axisymmetric 4 node quadrilateral structural elements (Plane42) in ANSYS Multiphysics, and axisymmetric constraints along the central axis, to allow movement in the axial direction only and subjected to a sinusoidal input displacement.

While nickel-titanium exhibits a highly non-linear super-elastic response, it was assumed that during ultrasound transmission and displacements in the range of interest, strains would remain less that .5 % and the material would remain in the austenitic phase, with a linear elastic response and modulus of 75 GPa. This assumption is evaluated by the model that can predict strains in the waveguide. The input material properties for the NiTi (from the manufacturer, Fort Wayne Metals©) wire waveguide are shown in Table1.

A harmonic response analysis was performed, as this would allow for the prediction of the waveguide resonant response over a range of frequencies. A sinusoidal input axial displacement was applied to the model over a set frequency range of 0 – 30 kHz. This input displacement was applied to the proximal elements of the wire model. From this harmonic analysis, the peak-to-peak displacements at the distal end of the modelled wire could be determined for all frequencies in the range of interest.

Initially, a mesh sensitivity analysis was performed to ensure sufficient resolution of the wave structure, so all resonant frequencies in the frequency range of interest were accurately resolved. Mesh density (pattern) is defined as the number of elements in the radial direction (r) multiplied by the number of elements in the axial direction (y) and is presented as (r × y) [include]. An insufficient number of elements in the axial direction will result in the internal mode shape being poorly resolved while the number of elements used in radial direction is adjusted to ensure good element shape and aspect ratios. The predicted resonant

frequencies over the frequency range of interest were compared with the analytical solution for the resonant frequencies of a thin rod subjected to a sinusoidal input [13].

Once an appropriate mesh structure was chosen, multiple models of wire waveguides, over a range of lengths from 118 mm – 303 mm, in steps of 5 mm, were generated to simulate the effects of different wire lengths on the distal tip displacements of the wire waveguide.

4.   Results and Discussion

4.1   *Experimental Results*

An example of an image obtained at the distal tip of an energised ultrasonic 1.0 mm diameter wire waveguide, with the optical microscope and image analysis software, is shown in *Figure 4*. The image clearly shows the streak of the vibrating tip and the superimposed measurement from the imaging analysis software. This process was repeated for a range of lengths of wire waveguide (118 mm – 303 mm) and *Figure 5* shows the results obtained for the axial peak-to-peak displacements at the distal tip of the waveguide, for various acoustic horn distal tip power levels.

These experimental results show clear evidence of which wire waveguide lengths exhibit a resonant response, and the effect of the wire waveguide length being close to a resonant length on the output displacements at the distal tip of the wire can be clearly seen. Experimental results at lengths approaching a resonant length could not be measured as it is a characteristic of the generator not to deliver power in this region. However, near the wire waveguide resonant length of 188 mm, a distal tip displacement of 98μm (p-p) at 17 Watts (RMS) input power was observed, while the distal tip displacement was only 46 μm (p-p) at the anti-resonant length of 143 mm.

Experimentally determined anti-resonance occurred at lengths of 143 mm, 218 mm and 288 mm (*see Figure 5*) and can be compared with the analytical solution for a thin rod subjected to a sinusoidal input [13]. This solution gives lengths, l_n, where resonance (*n = 1, 3, 5…*) and anti-resonance (*n = 2, 4, 6...*) occurs for a rod subjected to an input frequency, *f*, according to *Equation 1*.

$$l_n = \frac{nc}{4f} \tag{1}$$

where c is the speed of sound in the material.

For the material properties given in *Table 1* and a constant input frequency of *23.5 kHz*, the comparison between analytical results and the experimental results is given in *Table 2*. The location of the analytical anti-resonant lengths is also included in *Figures 5, 7 and 8*.

Despite the fact that the acoustic horn tip displacement, which is the input to the wire waveguide, cannot be measured directly, as an image with the optical microscope cannot be obtained within the casing, it is possible to infer the displacements applied by the distal tip of the acoustic horn to the wire waveguide for various input powers by observing the anti-resonant displacements achieved at these power levels. For example, the acoustic horn distal tip power level of 10 Watts (RMS) infers an applied peak-to-peak displacement of 32 μm to the proximal end of the wire waveguide and is shown as the line *AA* in *Figure 5*.

These results will form the input axial displacement to the harmonic numerical model. Also, the amplitudes near resonance and shape of the resonant peaks will allow for the determination of a damping value for the wire waveguide at the observed operating frequency of 23.5 kHz.

4.2   Numerical Results

The numerical results from a harmonic response analysis of a 1.0 mm diameter wire waveguide of 303 mm length, are shown in *Figure 6*, for a frequency range from 0 – 30 kHz and for an input displacement of 30 μm peak-to-peak. Two models with different mesh densities are shown and compared with the analytical solution of the resonant frequencies of a rod subjected to a sinusoidal input displacement [13]. It can be seen from *Figure 6* that an insufficient mesh density (1×10) results in the inaccurate determination of the higher resonant frequencies. The higher mesh density model (3×303) shows excellent comparison with the analytically determined resonant frequencies and is shown in *Table 3*.

Multiple models with this validated mesh density were developed to simulate a range of wire waveguide lengths from 118 mm – 303 mm and the distal tip peak-to-peak displacement results are shown in *Figure 7*. All results are taken at a frequency of 23.5 kHz and have input values of 32μm (p-p). These simulations were repeated for a number of constant damping values (4%, 4.5% and 5% shown).

The constant damping value is to account for all damping phenomena in the wire waveguide. This inputted damping value ζ is used to calculate the variable matrix stiffness multiplier β according to:

$$\beta = \frac{\zeta}{\pi f} \tag{2}$$

where f is the harmonic frequency range. This value is used by the finite element model to calculate the damping matrix $[C]$ according to:

$$[C] = (\beta)\,[K] \tag{3}$$

where $[K]$ is the structure stiffness matrix. The damping matrix is used in the general equation of motion for the structural system that is solved during an harmonic analysis:

$$[M](\ddot{u}) + [C](\dot{u}) + [K](u) = (F^a) \tag{4}$$

where $[M]$ is the structural mass matrix, $(\ddot{u})$ is the nodal acceleration vector, $(\dot{u})$ is the nodal velocity vector, (u) is the nodal displacement vector and (F^a) is the applied load vector.

The numerical results show the effect of resonance on the distal tip displacement of the wire waveguide and the lengths corresponding to resonance and anti-resonance compare favourably with those obtained from the analytical solution. The effect of damping is also noted and any model that is to be comparable with the actual experimental behaviour of the wire waveguide must have input peak-to-peak displacement, damping value and frequency of operation similar to the experimental apparatus.

In order to compare the experimental measurements with the numerical model of the wire waveguide, a number of models for a range of wire waveguide lengths (118mm - 303mm) were simulated for input displacements, frequency and damping as determined from the experimental results. Output distal tip displacements (p-p) were taken at a frequency of 23.5 kHz for two input displacements (p-p), 32μm and

46µm, corresponding to the acoustic horn distal tip power levels of 10 Watts (RMS) and 17 Watts (RMS) respectively.

These results are shown in *Figure 8* for a constant damping value of 4.5% and appear to fit the experimental data for both the wire waveguide distal tip peak-to-peak displacement and for the location of lengths where resonance and anti-resonance will occur and can simulate the overall behaviour of the wire waveguide over the range of lengths tested.

5. Conclusions

The therapeutic ultrasonic wire waveguide apparatus described satisfies the design criteria and is comparable with those described by other authors. Experimental measurements confirm that high amplitude peak-to-peak displacements of 98μm (p-p) can be delivered to the distal tip of the 1.0mm diameter NiTi wire waveguide at an operational frequency of 23.5 kHz.

The experimental work, in addition, shows the interrelationship at the lengths investigated between acoustic horn distal tip power, wire length and the wire waveguide distal tip peak-to-peak displacement. In particular, the experimental measurements show the critical effect of wire length on the output peak-to-peak displacements achieved as the wire waveguide length moves between resonant and anti-resonant lengths.

The numerical model that has been developed predicts this critical relationship and can determine wire waveguide resonant lengths and the peak-to-peak displacements over the range of lengths modelled. This model has been validated against experimental measurements, by the inclusion of a constant damping value for the NiTi waveguide of 4.5 %, and can be used to predict the behaviour of the apparatus over the range of wire waveguide lengths tested. The numerical model will prove a valuable design tool in the further development of therapeutic ultrasound waveguide technology.
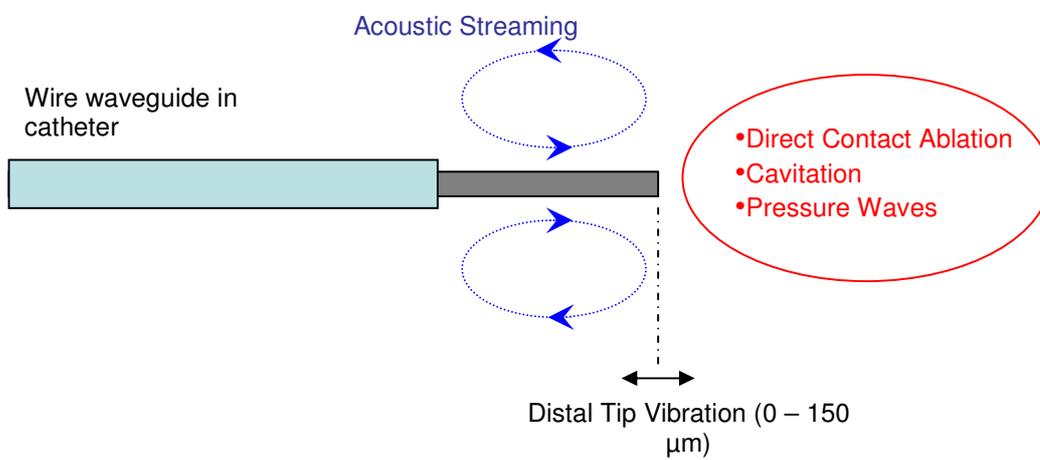
Figure 1: Location of disruption mechanisms of atherosclerotic plaque around ultrasonic vibrating distal-tip of waveguide in catheter
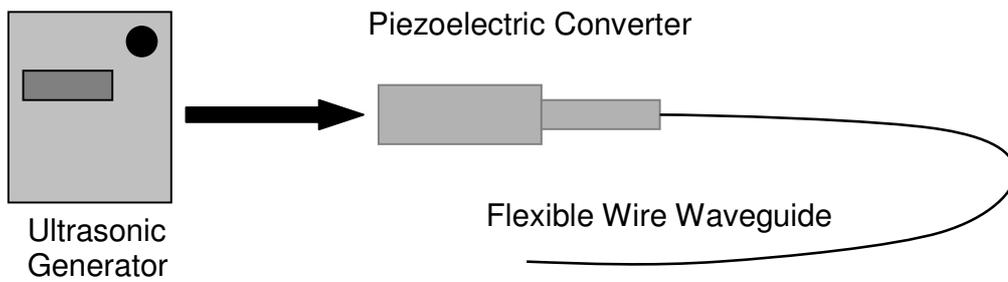
Figure 2: Schematic Diagram of therapeutic ultrasound wire waveguide apparatus showing ultrasonic generator, converter and wire waveguide
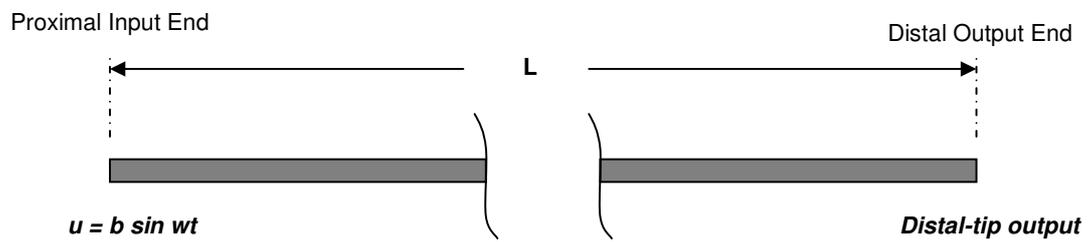
Proximal Input End

Distal Output End

L

u = b sin wt

Distal-tip output

Figure 3a: Problem sketch of wire waveguide, of length L, subjected to harmonic input displacement
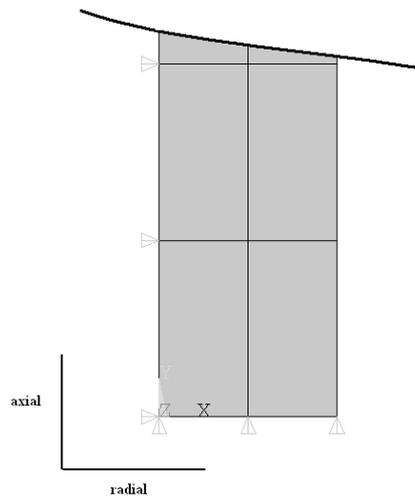
axial

radial

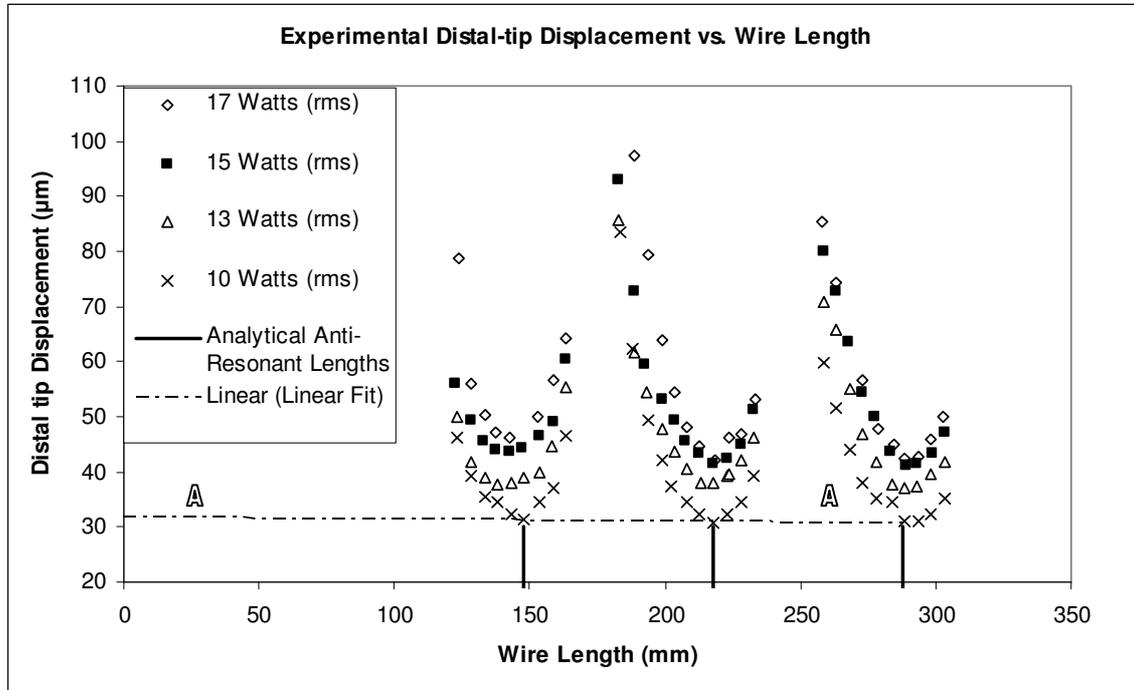**Figure 3b: Proximal end of waveguide model, showing radial and axial orientation.**
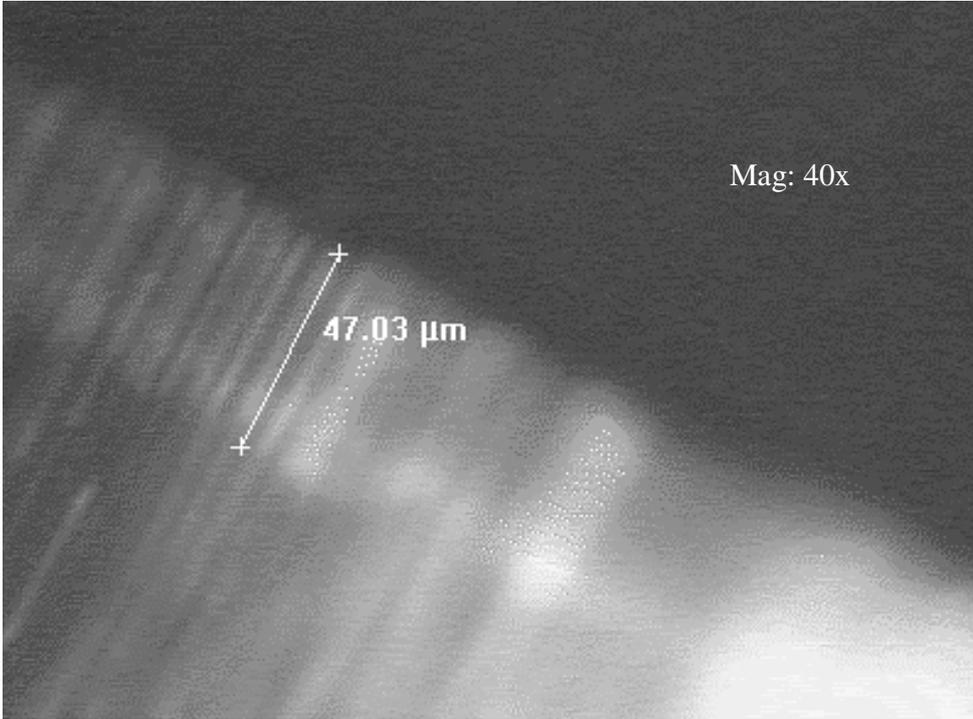
Figure 4: Image of vibrating distal-tip of the 1.0mm diameter wire waveguide

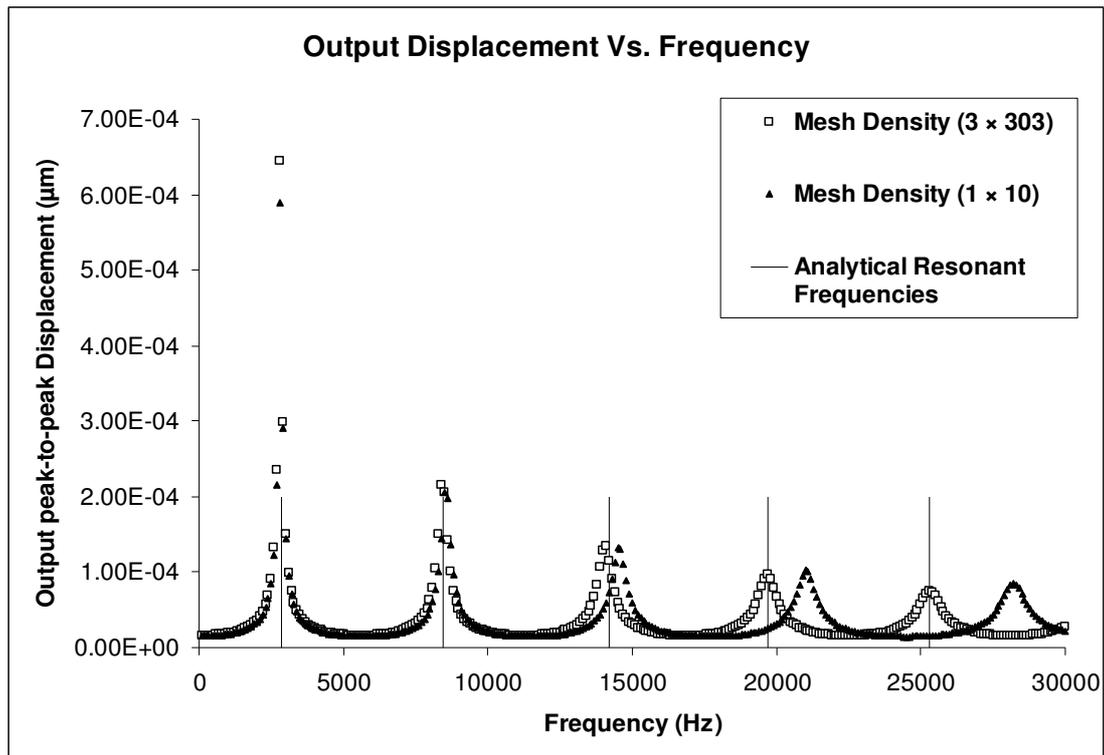**Experimental Distal-tip Displacement vs. Wire Length**

Figure 6: Numerical harmonic response results for output distal-tip displacement (p-p) for a frequency sweep of 0-30 kHz and an arbitrary constant damping value of 1.5%. Also shown are the analytically determined resonant frequencies.
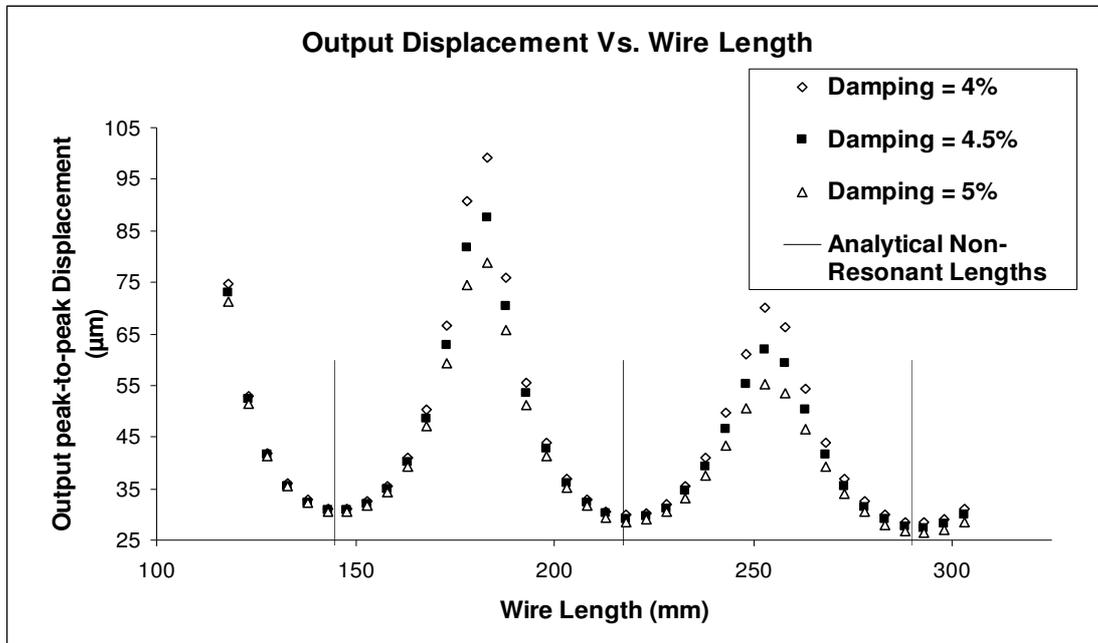
Figure 7: Numerical results of the output distal-tip displacements (p-p) for waveguides of various lengths (118- 303mm) for an input of 32 μm (p-p) at 23.5 kHz. Also shown are the analytically determined non-resonant lengths
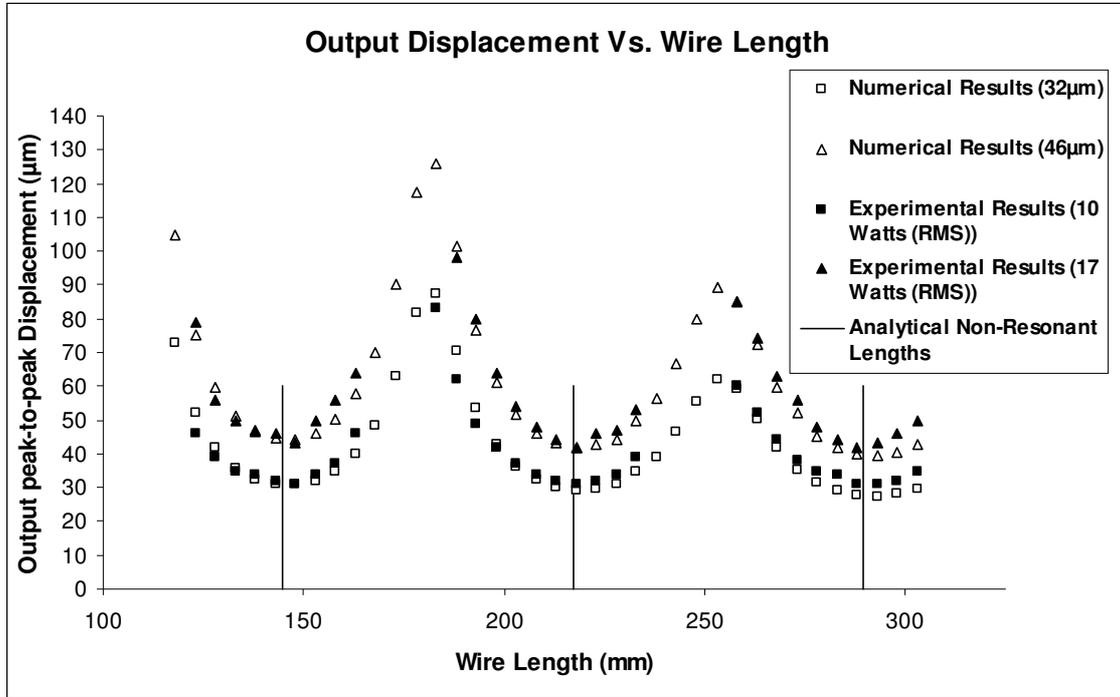
Figure 8: Comparison of numerical and experimental output distal tip peak-to-peak displacements for various wire lengths, at a frequency of 23.5 kHz and a damping value of 4.5%. Also shown, are the analytically determined anti-resonant lengths.

Table 1: Material properties for NiTi wire waveguide.

Property	(Units)
Young's Modulus	*75 (GPa)*
Density	*6450 (kg/m$^{3)}$)*
Poisson's Ratio	*0.32*

Table 2: Comparison of analytical and experimentally observed anti-resonant lengths of wire waveguide for *f=23.5 kHz*

Analytical Lengths (mm)	Experimental Lengths (mm)	Percentage Error (%)
144.8 (n=4)	*143*	*1.24*
217.2 (n=6)	*218*	*0.36*
289.6 (n=8)	*288*	*0.55*

Table 3: Comparison of analytical and numerically predicted resonant frequencies of wire waveguide for *l =303 mm*

Analytical Resonant Frequencies (Hz)	Numerical Resonant Frequencies (Hz)	Percentage Error (%)
2,840 (n=1)	*2,813*	*0.96*
8,438 (n=3)	*8,440*	*0.029*
14,204 (n=5)	*14,067*	*0.95*
19,688 (n=7)	*19,695*	*0.03*
25,314 (n=9)	*25,324*	*0.03*

References

[1]   Yock PG and Fitzgerald PJ. Catheter-based ultrasound thrombolysis: Shake, rattle and reperfuse. Circulation 1997; 95: 1360- 62.

[2]   Rosenschein U, Bernstein J, Di Segni E, Kaplinsky E, Bernheim J, Rozenszain LA. Experimental Ultrasonic Angioplasty: disruption of atherosclerotic plaques and thrombi in vitro and arterial recanalisation in vivo. J Am Coll Cardiol 1990; 15: 711-17.

[3]   Siegel RJ, Gunn J, Ahsan A, Fishbein MC, Bowes RJ, Oakley D, Wales C, Steffen W, Campbell S, Nita H, Mills T, Silverton P, Myler RK, Cumberland DC.   Use of Therapeutic Ultrasound in Percutaneous Coronary Angioplasty, Experimental in vitro studies and initial clinical experience. Circulation 1994; 89(4): 1587- 92.

[4]   Topoleski LDT, Salunke NV. Mechanical behaviour of calcified plaques: a summary of compression and stress-relaxation experiments. Z Kardiol 2000; 89(2): 85- 91.

[5]   Sobbe A, Stumpff U, Trubenstein G, Figge H, Kozuschek W. Die Ultraschall-Auflosung von Thromben. Klin Wochenschr 1974; 52: 1117- 21.

[6]   Siegel RJ, Fishbein MC, Forrester J, Moore K, DeCastro E, Daykhovsky Z, Don Michael TA Ultrasonic Plaque Ablation: a new method for recanalisation of partially or totally occluded arteries. Circulation 1988; 78: 1443- 1448.

[7]   Rosenschein U, Rozenszajn LA, Kraus L, Marboe CC, Watkins JF, Rose EA, David D, Cannon PJ, Weinstein JS. Ultrasound Angioplasty in Totally Occluded Peripheral Arteries. Circulation 1991; 83: 1976- 1986.

[8] Fischell TA, Abbas MA, Grant GW, Siegel RJ. Ultrasonic Energy: Effects on vascular function and integrity. Circulation 1991; 84: 1783 -95.

[9] Ariani M, Fishbein MC, Chae JS, Sadeghi H, Don Michael TA, Dubin SB, Siegel RJ. Dissolution of Peripheral Arterial Thrombi by Ultrasound. Circulation 1991; 84: 1680- 1688.

[10] Demer LL, Mehrdad A, Seigel RJ. High Intensity Ultrasound Increases Distensibility of Calcific Atherosclerotic Arteries. JACC 1991; 18(5): 1259-1262.

[11] United States Patent No: US5304115. SONICSTAR INTERNATIONAL LTD and BAXTER INT. Ultrasonic angioplasty device incorporating improved transmission member and ablation probe. 1994.

[12] Atar S, Luo H, Nagai T, Siegel RJ. Ultrasonic Thrombolysis: catheter-delivered and transcutaneous applications. European Journal of Ultrasound 1999; 9: 39-54.

[13] Steidel RF(Jr). An Introduction to Mechanical Vibrations, 3rd Edition, Wiley, 1989.

[14] ANSYS© Help Files. ANSYS© Multiphysics, Version 8.1.